Ab initio shell model for $A=10$ nuclei

E. Caurier,[1] P. Navrátil,[2] W. E. Ormand,[2] and J. P. Vary[3]
[1]*Institut de Recherches Subatomiques (IN2P3-CNRS-Université Louis Pasteur), Batiment 27/1, 67037 Strasbourg Cedex 2, France*
[2]*Lawrence Livermore National Laboratory, L-414, P.O. Box 808, Livermore, California 94551*
[3]*Department of Physics and Astronomy, Iowa State University, Ames, Iowa 50011*
(Received 10 May 2002; published 13 August 2002)

We investigate properties of $A=10$ nuclei in the *ab initio*, no-core shell model using realistic Argonne and CD-Bonn nucleon-nucleon (NN) potentials and basis spaces through $9\hbar\Omega$ (with basis dimensions reaching 5.5×10^8). Results for binding energies, excitation spectra (including negative parity and $2\hbar\Omega$-dominated intruder states), electromagnetic properties, and the isospin-mixing correction of the $^{10}\mathrm{C}\rightarrow{}^{10}\mathrm{B}$ Fermi transition are presented. For ^{10}B, these NN potentials produce a $J^\pi T=1^+0$ ground state, contrary to the experimental 3^+0, a clear indication of the need for true three-body forces.

DOI: 10.1103/PhysRevC.66.024314 PACS number(s): 21.60.Cs, 21.10.Dr, 21.30.Fe, 27.20.+n

I. INTRODUCTION

Various methods can be used to solve systems of more than two nucleons interacting by realistic interactions [1–3]. For $A>4$ systems, a prominent approach has been the Green's function Monte Carlo (GFMC) method [2]. An alternative, and complementary, approach is the no-core shell model (NCSM) [3–9], which is based on effective interactions within the framework of a finite Hilbert space. In this case, one derives an effective interaction for the A-body system within a computationally tractable basis space using a method designed to converge towards the exact result.

The applications of NCSM to date have been performed for both the $0s$- and the $0p$-shell nuclei in large, multi-$\hbar\Omega$ basis spaces. Initial investigations used two-body interactions based on a G-matrix approach [4], while later, the Lee-Suzuki procedure [10] was implemented to derive two-body effective interactions for the NCSM [5]. The earlier G-matrix approach used a phenomenological parameter Δ that lacked a clear physical motivation. In addition, the G matrix is non-Hermitian and Hermiticity was restored by a phenomenological averaging procedure in many initial investigations. The application of the Lee-Suzuki procedure eliminated these approximations [5]. A currently used formulation was presented in Ref. [6] where convergence to exact solutions was demonstrated for the $A=3$ system. Later, the same was accomplished for the $A=4$ system [7] and it was also shown that a three-body effective interaction improves the convergence of the method.

The optimum strategy for the NCSM is to employ the largest model space possible with the largest number of clusters derived in the effective interaction. Naturally, computational limitations require a compromise in the size of the model space and the clusters used in the effective interaction. Recently, three-body effective interactions have been applied in the NCSM for nuclei with $A\leqslant10$ [9]. Computational restrictions limited these calculations to $4\hbar\Omega$, and it seems feasible to extend them to $6\hbar\Omega$ in the future. On the other hand, current technology permits larger-scale calculations when implementing only two-body effective interactions, for example the NCSM has recently been applied to $A\leqslant8$ for model spaces extending to $10\hbar\Omega$ [8]. As a complementary approach that will also help to elucidate the advantages of the various strategies, we report here the results of our recent efforts to extend the model space up to $8-9\hbar\Omega$ for $A=10$.

It is interesting to study $A=10$ nuclei in *ab initio* approaches for several reasons. These nuclei have a rich structure with both positive and negative parity bound states. There are experimental candidates for the intruder states. It is also important to study the isospin-mixing correction for the $^{10}\mathrm{C}\rightarrow{}^{10}\mathrm{B}$ Fermi transition, which is relevant for the investigation of the unitarity condition of the CKM matrix. Finally, the GFMC method is now being applied to $A=10$ nuclei, so it is interesting to compare the NCSM and the GFMC predictions.

In Sec. II, we discuss our NCSM formulation, i.e., the Hamiltonian and effective interaction framework. Results for the $A=10$ systems interacting by the CD-Bonn and the Argonne V8′ NN potentials are given in Sec. III. We discuss the binding energies, excitation spectra, electromagnetic (EM) properties, as well as Gamow-Teller transitions. The isospin-mixing correction for the $^{10}\mathrm{C}\rightarrow{}^{10}\mathrm{B}$ Fermi transition is discussed in Sec. III E. In Sec. IV, we present concluding remarks.

II. *Ab initio* NO-CORE SHELL MODEL

The NCSM approach in the form applied in this paper was presented recently, e.g., in Ref. [3]. To make the present paper self-contained, we repeat the basic steps of the method in this section.

A. Hamiltonian

In the NCSM approach we start from the intrinsic Hamiltonian for the A-nucleon system, i.e.,

$$H_A=T_{\mathrm{rel}}+\mathcal{V}=\frac{1}{A}\sum_{i<j}^{A}\frac{(\vec{p}_i-\vec{p}_j)^2}{2m}+\sum_{i<j=1}^{A}V_{\mathrm{N}}(\vec{r}_i-\vec{r}_j), \quad (1)$$

where m is the nucleon mass and $V_{\mathrm{N}}(\vec{r}_i-\vec{r}_j)$, the NN interaction, both strong and electromagnetic components. It is purely a two-body operator without a phenomenological single-particle potential. At present, we examine only realis-

tic two-body *NN* potentials, and extensions to include three-body *NNN* interactions are underway.

We may use both coordinate-space *NN* potentials, such as the Argonne potentials [2] or momentum-space dependent *NN* potentials, such as the CD-Bonn [11]. In the next step we modify the Hamiltonian (1) by adding to it the center-of-mass (c.m.) HO Hamiltonian $H_{\rm c.m.}=T_{\rm c.m.}+U_{\rm c.m.}$, where $U_{\rm c.m.}=\frac{1}{2}Am\Omega^2\vec{R}^2$, $\vec{R}=1/A\Sigma_{i=1}^{A}\vec{r}_i$. The effect of the HO c.m. Hamiltonian will later be subtracted out in the final many-body calculation so there is no net influence on intrinsic properties of the many-body system. In fact, in the infinite space such a potential has no influence on the intrinsic properties at all. However, this added/subtracted potential facilitates the use of the convenient HO basis for evaluating the effective interactions. The modified Hamiltonian, with a pseudodependence on the HO frequency Ω, can be cast into the form

$$H_A^{\Omega}=H_A+H_{\rm c.m.}=\sum_{i=1}^{A}\left[\frac{\vec{p}_i^{\,2}}{2m}+\frac{1}{2}m\Omega^2\vec{r}_i^{\,2}\right]+\sum_{i<j=1}^{A}\left[V_{\rm N}(\vec{r}_i-\vec{r}_j)-\frac{m\Omega^2}{2A}(\vec{r}_i-\vec{r}_j)^2\right]. \tag{2}$$

Since we solve the many-body problem in a finite HO basis space, the realistic nuclear interaction in Eq. (2) will yield pathological results unless we use it to derive a model-space dependent effective Hamiltonian. In general, for an *A*-nucleon system, an *A*-body effective interaction is needed. In the present calculations, we make use of a two-body cluster approximation for the effective interaction. Large model spaces are desirable to minimize the role of neglected effects, which a larger cluster would include.

As the Hamiltonians H_A (1) and H_A^{Ω} (2) differ only by a c.m. dependent term, no dependence on Ω should exist for the intrinsic properties of the nucleus. However, because of the less-than-*A*-body-cluster approximation for the effective interaction, a dependence on Ω arises in our results. This dependence on Ω and on the size of the basis space provides measures of the severity of this approximation.

B. Two-body effective interaction and the basis space definition

In order to derive the effective interaction, we employ the Lee-Suzuki similarity transformation method [10,12], which yields an Hermitian effective interaction. The approach presented here leads to the same two-body effective interaction as used in our previous papers [3,6–8].

Let us write the Hamiltonian (2) schematically as

$$H_A^{\Omega}=\sum_{i=1}^{A}h_i+\sum_{i<j=1}^{A}V_{ij}. \tag{3}$$

In the spirit of Da Providencia and Shakin [13] and Lee, Suzuki and Okamoto [10,12], we introduce a unitary transformation of the Hamiltonian, which is able to accommodate the short-range two-body correlations in a nucleus, by choosing an antihermitian operator *S*, such that

$$\mathcal{H}=e^{-S}H_A^{\Omega}e^{S}. \tag{4}$$

In our approach, *S* is determined by the requirements that $\mathcal{H}$ and H_A^{Ω} have the same symmetries and eigenspectra over the subspace $\mathcal{K}$ of the full Hilbert space. In general, both *S* and the transformed Hamiltonian are *A*-body operators. Our simplest, yet nontrivial approximation to $\mathcal{H}$ is to develop a two-body effective Hamiltonian (i.e., $a=2$, where *a* represents the cluster number and in effect substitutes for *A* in the sums of the above equations). The next improvement is to develop a three-body effective Hamiltonian ($a=3$). This approach consists then of an approximation to a particular level of clustering ($a\leqslant A$):

$$\mathcal{H}=\mathcal{H}^{(1)}+\mathcal{H}^{(a)}, \tag{5}$$

where the one-body and *a*-body pieces are given as

$$\mathcal{H}^{(1)}=\sum_{i=1}^{A}h_i, \tag{6a}$$

$$\mathcal{H}^{(a)}=\frac{\binom{A}{2}}{\binom{A}{a}\binom{a}{2}}\sum_{i_1<i_2<\cdots<i_a}^{A}\tilde{V}_{i_1i_2\cdots i_a}, \tag{6b}$$

with

$$\tilde{V}_{12\cdots a}=e^{-S^{(a)}}H_a^{\Omega}e^{S^{(a)}}-\sum_{i=1}^{a}h_i, \tag{7}$$

where $S^{(a)}$ is an *a*-body operator and

$$H_a^{\Omega}=\sum_{i=1}^{a}h_i+\sum_{i<j}^{a}V_{ij}. \tag{8}$$

Note that there is no sum over "*a*" in Eq. (5), and that a perturbative expansion in terms of one-body, two-body, etc., clusters is not possible.

If the full *A*-body space is divided into an active (*P*) model space and an excluded (*Q*) space, using the projectors *P* and *Q* with $P+Q=1$, it is possible to determine the transformation operator S_a from the decoupling condition

$$Q_ae^{-S^{(a)}}H_a^{\Omega}e^{S^{(a)}}P_a=0, \tag{9}$$

and the simultaneous restrictions $P_aS^{(a)}P_a=Q_aS^{(a)}Q_a=0$. Note that *a*-nucleon-state projectors (P_a,Q_a) appear in Eq. (9) and are applied to the *a*-nucleon states $|\alpha\rangle$, which effectively define the *a*-cluster matrix elements used in the *A*-body calculation.

The unitary transformation and decoupling condition, introduced by Suzuki and Okamoto and referred to as the unitary-model-operator approach (UMOA) [14], has the solution

$$S^{(a)}=\operatorname{arctanh}(\omega-\omega^{\dagger}), \tag{10}$$

with ω satisfying $\omega=Q_a\omega P_a$. Furthermore, we also have

$$Q_a e^{-\omega} H_a^{\Omega} e^{\omega} P_a = 0. \tag{11}$$

With Eq. (10), we have for the a cluster

$$\overline{H}_{a\text{-eff}} = (P_a + \omega^\dagger \omega)^{-1/2} (P_a + P_a \omega^\dagger Q_a) \times H_a^{\Omega} (Q_a \omega P_a + P_a)(P_a + \omega^\dagger \omega)^{-1/2}. \tag{12}$$

If the eigensolutions of the Hamiltonian H_a^{Ω} are given by $H_a^{\Omega}|k\rangle = E_k|k\rangle$, then the operator ω can be determined as

$$\langle \alpha_Q|\omega|\alpha_P\rangle = \sum_{k\in\mathcal{K}} \langle \alpha_Q|k\rangle\langle\tilde{k}|\alpha_P\rangle, \tag{13}$$

where $|\alpha_P\rangle$ and $|\alpha_Q\rangle$ denote the a-nucleon model- and Q-space basis states, respectively. The tilde in Eq. (13) denotes the inverted matrix $\langle \alpha_P|k\rangle$, i.e., $\Sigma_{\alpha_P}\langle\tilde{k}|\alpha_P\rangle\langle\alpha_P|k'\rangle = \delta_{k,k'}$ and $\Sigma_k\langle\alpha'_P|\tilde{k}\rangle\langle k|\alpha_P\rangle = \delta_{\alpha'_P,\alpha_P}$, for $k,k' \in \mathcal{K}$. Note the sum $\mathcal{K}$ denotes a set of d_P eigenvectors whose properties are exactly reproduced in the model space, with d_P equal to the dimension of the model space.

With the help of the solution for ω (13) we obtain a simple expression for the matrix elements of the Hermitian effective Hamiltonian

$$\langle \alpha_P|\overline{H}_{a\text{-eff}}|\alpha'_P\rangle = \sum_{k\in\mathcal{K}} \sum_{\alpha''_P} \sum_{\alpha'''_P} \langle \alpha_P|(P_a + \omega^\dagger\omega)^{-1/2}|\alpha''_P\rangle \times \langle \alpha''_P|\tilde{k}\rangle E_k \langle\tilde{k}|\alpha'''_P\rangle \times \langle \alpha'''_P|(P_a + \omega^\dagger\omega)^{-1/2}|\alpha'_P\rangle. \tag{14}$$

For computation of the matrix elements of $(P_a + \omega^\dagger\omega)^{-1/2}$, we use the relation

$$\langle \alpha_P|(P_a + \omega^\dagger\omega)|\alpha''_P\rangle = \sum_{k\in\mathcal{K}} \langle \alpha_P|\tilde{k}\rangle\langle\tilde{k}|\alpha''_P\rangle. \tag{15}$$

We note that in the limit $a \to A$, we obtain the exact solutions for d_P states of the full problem for any finite basis space, with flexibility for choice of physical states subject to certain conditions [15].

Now, we introduce our present application, in which we take $a=2$. Let us write explicitly the two-nucleon Hamiltonian in the relative and c.m. coordinates, e.g.,

$$H_{a=2}^{\Omega} = H_{02} + H_{2\text{c.m.}} + V_{12} = \frac{\vec{p}^{\,2}}{2m} + \frac{1}{2} m\Omega^2 \vec{r}^{\,2} + H_{2\text{c.m.}} + V_{\text{N}}(\sqrt{2}\vec{r}) - \frac{m\Omega^2}{A}\vec{r}^{\,2}, \tag{16}$$

where $H_{02} + H_{2\text{c.m.}} = h_1 + h_2$, $\vec{r} = \sqrt{\frac{1}{2}}(\vec{r}_1 - \vec{r}_2)$, and $\vec{p} = \sqrt{\frac{1}{2}}(\vec{p}_1 - \vec{p}_2)$. The two-nucleon problem is then solved in a relative HO basis space with high precision. The c.m. motion of the two nucleons is not affected by the transformation $S^{(2)}$. The term $H_{2\text{c.m.}}$ does not contribute to the effective interaction calculation and cancels out as seen in Eq. (7). The A in Eq. (16) is set to 10 in the present application.

The relative-coordinate two-nucleon HO states used in the calculation are characterized by quantum numbers $|nlsjt\rangle$ with the radial and orbital HO quantum numbers corresponding to coordinate $\vec{r}$ and momentum $\vec{p}$, respectively. Typically, we solve the two-nucleon Hamiltonian in Eq. (16) for all two-nucleon channels up through $j=6$. For the channels with higher j we take V_N to be zero. Thus, only the relative kinetic term contributes in such channels in the many-nucleon calculation.

The model space P_2 is defined by the maximal number of allowed HO excitations of the A-nucleon system N_{totmax} from the condition $2n+l \leq N_{\text{totmax}} - N_{\text{spsmin}}$, where N_{spsmin} denotes the minimal possible value of the HO quanta of the spectators, i.e., nucleons not affected by the interaction process. For, e.g., ^{10}B, $N_{\text{spsmin}}=4$ as there are 6 nucleons in the $0p$ shell in the unperturbed ground-state configuration and, e.g., $N_{\text{totmax}} = N_{\text{spsmin}} + 2 + N_{\max}$, where $N_{\max}$ represents the maximum HO quanta of the many-body excitation above the unperturbed ground-state configuration. For ^{10}B, $N_{\text{totmax}} = 12$ for an $N_{\max}=6$ or "$6\hbar\Omega$" calculation.

In order to construct the operator ω we need to select the set of eigenvectors $\mathcal{K}$. In the present application we select the lowest states obtained in each two-body channel. It turns out that these states also have the largest overlap with the model space for the range of $\hbar\Omega$ we investigate and the P spaces we select. Their number is given by the number of basis states satisfying $2n+l \leq N_{\text{totmax}} - N_{\text{spsmin}}$.

Finally, the two-body effective interaction is determined from the two-nucleon effective Hamiltonian, obtained from Eq. (14), as $V_{2\text{eff}} = P_2 \tilde{V}_{12} P_2 = P_2(\overline{H}_{2\text{eff}} - h_1 - h_2)P_2$. Apart from being a function of the nucleon number A, $V_{2\text{eff}}$ depends on the HO frequency Ω and on the parameter N_{totmax}, defining the basis space. It has the important property that $V_{2\text{eff}} \to V_{12}$ for $N_{\text{totmax}} \to \infty$, following from the fact that $\omega \to 0$ for $P \to 1$. We note that $\mathcal{H}^{(1)} + \mathcal{H}^{(2)} - H_{\text{CM}}$ is translationally invariant. We note that in adition to NCSM the Lee-Suzuki method has also been applied in an analogous way within the Jacobi-coordinate hyperspherical harmonics method [16].

C. Solution of the many-body Schrödinger equation

Once the two-nucleon effective interaction is derived and transformed from the relative coordinate basis to the single-particle coordinate basis, we evaluate and diagonalize the effective Hamiltonian in an A nucleon (N neutron and Z proton) Slater determinant HO basis that spans a complete $N_{\max}\hbar\Omega$ space. This choice of the basis together with the fact that the effective Hamiltonian is translationally invariant guarantees the factorization of each of our wave functions into a product of a c.m. $\frac{3}{2}\hbar\Omega$ wave function and a wave function corresponding to the internal motion. Due to this property, it is straightforward to remove c.m. effects exactly from all observables. We note that only a nonredundant subset of the Slater determinant states are needed to span the translationally invariant A-nucleon P space, and we isolate this subset by adding a term $\Lambda(H_{\text{c.m.}} - \frac{3}{2}\hbar\Omega)$ to the effective

Hamiltonian with, e.g., $\Lambda = 10$. This procedure moves the states with excited c.m. motion correspondingly higher in the calculations and away from the physically relevant states all of which have a (passive) $0S$ state of c.m. motion. Due to the translational invariance of our approach, the physical eigenenergies and other observables are independent of Λ.

The evaluation of the A-nucleon Hamiltonian and its diagonalization is a highly nontrivial problem due to very large dimensions we encounter. In the present work, we performed the many-body calculation with two completely independent shell model codes. First, we used a newly developed version of the code ANTOINE [17]. Second, we employed the many-fermion dynamics (MFD) shell-model code [18] used in the previous NCSM investigations. Both codes work in the m scheme for basis spaces comprising many major shells and use the Lanczos diagonalization algorithm. The ANTOINE code allows a sophisticated selection of the pivot vector first by diagonalizing $\hat{J}^2$ in a small model space and second by using the eigenvectors from smaller model spaces as pivots for the larger model spaces. This reduces the number of Lanczos iterations needed for the convergence of the lowest states. Also, the algorithm for the calculation of the Hamiltonian matrix elements is very efficient due to a special basis ordering that allows a very fast generation of all the nonzero matrix elements, which are obtained with just three integer additions. The MFD code, on the other hand, is parallelized using MPI and runs efficiently on parallel machines. It allows one to compute many Lanczos iterations needed to obtain higher lying states and their properties. Also, the wave functions obtained by the MFD can be further processed by a parallelized code that we developed to obtain, e.g., one- and two-body transition densities.

We note that the ANTOINE code has been under development since 1989 [17] and its algorithms have been highly optimized for running on a single processor machine such as a scientific workstation. The MFD has been under development since 1992 [18] as a general purpose code for a variety of fermionic systems and its algorithms have been highly optimized for running on parallel machines. These codes have been developed independently by different groups and different algorithms are involved. Hence, the agreement reported here and elsewhere [8] to within machine precision of results from the ANTOINE and the MFD is significant.

III. $A = 10$ RESULTS

We performed calculations up through the $6\hbar\Omega$ basis spaces, with dimensions $N_D = 1.2 \times 10^7$, using both codes and cross checked that the same results were obtained. The calculations in the larger spaces up through the $9\hbar\Omega$ ($N_D \approx 5.5 \times 10^8$) were performed only using the ANTOINE code.

We present results obtained using the nonlocal CD-Bonn [11] NN potential and the local Argonne V8′ [2] NN potential, which is an isospin invariant and slightly truncated version of the AV18 NN potential. The Coulomb interaction was included. The use of the AV8′ is advantageous since some preliminary results are available for this potential with the Green's function Monte Carlo (GFMC) method for $A = 10$ [19].

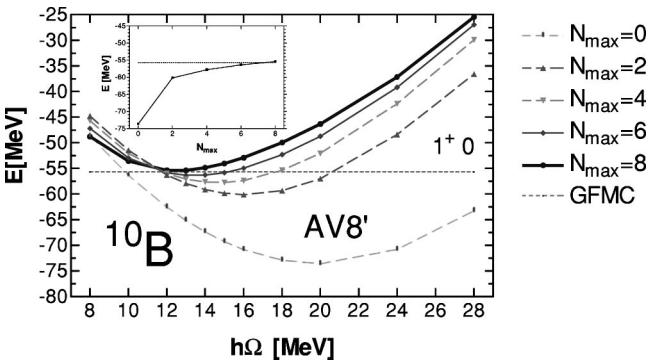

FIG. 1. ^{10}B ground-state energy dependence on the HO frequency for the $0-8\hbar\Omega$ model spaces calculated using the effective interaction derived from the AV8′ NN potential with Coulomb included. The GFMC result is from Ref. [19]. In the inset, the ground-state energies at the HO frequency minima as a function of $N_{\max}$ are plotted.

We also investigate electromagnetic and weak transitions. Throughout this study, we employ traditional one-body transition operators with the free nucleon charges. We note that due to the factorization of our wave functions into a product of the intrinsic and the $\frac{3}{2}\hbar\Omega$ c.m. component we obtain translationally invariant transition matrix elements for the observables we investigate here. In general, it is possible to correct for the c.m. motion for any observable within our formalism. As we work in a truncated basis space, the transition operators should also be renormalized through a well-controlled theoretical framework. The relevant method was discussed in Ref. [3]. To compute a two-body correction to the one-body operator is more involved than the evaluation of the effective interaction, however. This complexity arises because the transformation from relative plus c.m. coordinates to single-particle coordinates is needed in a sufficiently large two-nucleon space typically comprising excitations up to several hundred $\hbar\Omega$. In the present study, we do not calculate this correction. It will be a subject of our future work. Here, rather, we investigate the basis size dependence of the observables that gives us a good impression of the extent of the needed renormalization.

A. ^{10}B

As our method depends on the basis-space size and the HO frequency, we first performed investigations of the lowest states of the $A = 10$ nuclei in basis spaces from $0\hbar\Omega$ through $8\hbar\Omega$ ($1\hbar\Omega$ through $9\hbar\Omega$) for the positive- (negative-) parity states and for the HO frequency range $\hbar\Omega = 8 - 28$ MeV. In Figs. 1 and 2, the dependence for the $1^+_1 0$ state of ^{10}B obtained using the AV8′ and the CD-Bonn 2000 NN potentials, respectively, is shown. We seek a region where the eigenenergy is approximately independent of the HO frequency. This behavior is found in the largest model space in the range of about $\hbar\Omega = 12 - 15$ MeV and we select $\hbar\Omega = 14$ MeV for our detailed investigations of the excited states. In general, we obtain a better convergence rate and a weaker HO frequency dependence for the CD-Bonn NN potential. For both potentials, even though full convergence is

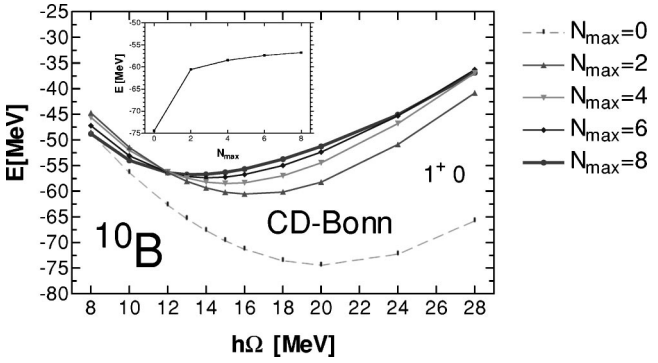

FIG. 2. ^{10}B ground-state energy dependence on the HO frequency for the $0-8\hbar\Omega$ model spaces calculated using the effective interaction derived from the CD-Bonn 2000 *NN* potential. In the inset, the ground-state energies at the HO frequency minima as a function of $N_{\max}$ are plotted.

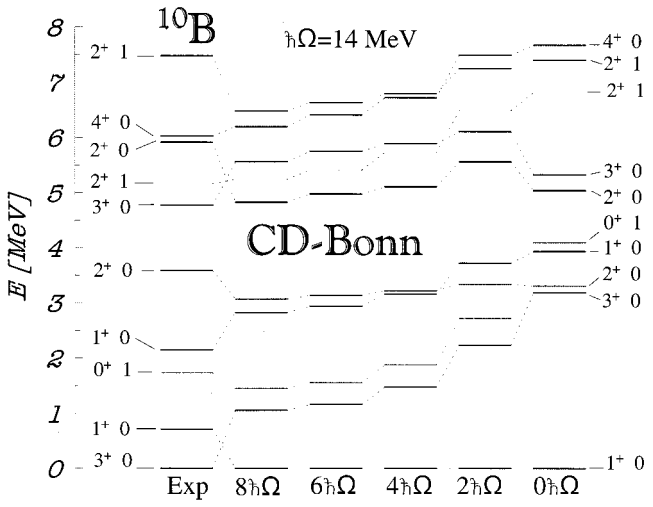

FIG. 3. Experimental and theoretical positive-parity excitation spectra of ^{10}B. Results obtained in $0-8\hbar\Omega$ model spaces are compared. The effective interaction was derived from the CD-Bonn 2000 *NN* potential in a HO basis with $\hbar\Omega=14$ MeV. The experimental values are from Ref. [20].

not quite achieved, we observe the convergence behavior as both the HO frequency dependence becomes weaker and, as discussed later, the relative differences in the excitation spectra are smaller with increasing basis size.

To better judge this convergence pattern, we plot in the insets of Figs. 1 and 2 the $N_{\max}$ dependence of the energies at the minima of the HO frequency curves. For the AV8′ calculation, we compare with the GFMC results [19]. In Table I, we summarize the lowest eigenenergy results. For ^{10}B with AV8′, we obtained a reasonable agreement with the GFMC results. We note that our CD-Bonn binding energies are about 1.5–2 MeV larger than the corresponding AV8′ results and that both potentials underbind by as much as 10 MeV when compared to experiment.

In Fig. 3, we present the ^{10}B excitation spectrum for the basis spaces from $0\hbar\Omega$ to $8\hbar\Omega$ obtained using the CD-Bonn 2000 *NN* potential and the selected HO frequency of $\hbar\Omega=14$ MeV. We observe a strong indication of convergence, namely, that the differences in the spectra decrease and the level stability increases with larger $N_{\max}$. We can see that our calculation predicts the 1^+0 ground state contrary to the experimental 3^+0. To shed more light on this issue, we present the complete HO frequency dependence of the 1^+0 and the 3^+0 state energies as obtained in the $4\hbar\Omega$ and the $8\hbar\Omega$ spaces in Fig. 4. Apparently, the two states do cross at some higher frequencies. However, over the region of the least $\hbar\Omega$ dependence, the 1^+0 state is consistently below the 3^+0 state. More importantly, as $N_{\max}$ increases, the range of frequencies with 1^+0 as the ground state increases. Thus, we conclude that both the Argonne and the CD-Bonn *NN* potentials predict the 1^+0 state as the ground state of ^{10}B, which is in disagreement with the experimental observation of 3^+0 ground state. This fact, in addition to the underbinding, is a very strong indication for the need of multinucleon forces. This level reversal has also been confirmed in the GFMC calculations for the Argonne potentials (see Table I), and is likely due to an insufficient spin-orbit interaction present in the realistic *NN* potentials. Furthermore, prelimenary calculations that include a real three-body force indicate that both the total binding energy as well as the level ordering can be brought to agreement with experiment [19]. We also note

TABLE I. The NCSM results at the HO frequency minima in the $8(9)\hbar\Omega$ basis space for the ground-state (lowest negative-parity-state) energies, in MeV, of ^{10}B, ^{10}Be, ^{10}C, ^{10}Li, and ^{10}He using the AV8′ and the CD-Bonn *NN* potentials with Coulomb included. The GFMC results for the AV8′ [19] are shown for comparison. We note the NCSM is not a variational calculation. Thus, more binding does not necessarily imply a better result.

	$AV8'_{GFMC}$	$AV8'_{NCSM}$	CD-Bonn$_{NCSM}$	Exp
^{10}B (1^+0)	−55.67(26)	−55.37	−56.75	−64.033
^{10}B (3^+0)	−53.23(26)	−53.83	−55.63	−64.751
^{10}B (2^-0)		−48.53	−49.82	−59.641
^{10}Be (0^+1)	−56.11(20)	−55.35	−57.06	−64.977
^{10}Be (1^-1)		−48.45	−49.68	−59.017
^{10}C (0^+1)		−50.87	−52.33	−60.321
^{10}Li (0^+2)		−36.12	−36.82 (1^+2)	−45.316 $(?^?2)$
^{10}He (0^+3)		−21.93	−22.14	−30.340

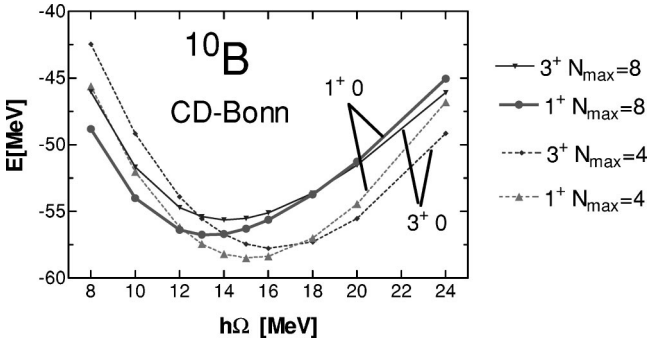

FIG. 4. ^{10}B 1^+0 and 3^+0 state energy dependence on the HO frequency for the $4\hbar\Omega$ and $8\hbar\Omega$ model spaces calculated using the CD-Bonn 2000 *NN* potential.

that this situation is similar to other calculations we have performed using *G*-matrix based effective interactions for the *sd*-shell nucleus ^{22}Na, which fail to predict the experimental ground state spin.

We also investigated the electromagnetic transitions as well as the quadrupole and magnetic moments of the lowest ^{10}B levels. Results obtained using the CD-Bonn *NN* potential at the optimal HO frequency of $\hbar\Omega = 14$ MeV are presented in Table II. To judge the stability and the trends of our results, the dependence on the basis size in the $4-8\hbar\Omega$ range is shown. The calculated magnetic moments of the 3_1^+0 and the 1_1^+0 states are stable and in a reasonable agreement with experiment. The 3_1^+0 quadrupole moment shows a steady increase with the basis size but even in the $8\hbar\Omega$ basis space the experimental value is underestimated by about 16%. Here, we used free nucleon charges and no operator renormalization due to basis-space truncation. The sensitivity of basis size on our $E2$ results suggest the need to employ effective transition operators, which may be evaluated within the present framework and will be a topic for future work. Our results for the transitions to the 1_1^+0 and the 3_1^+0 states indicate an inadequate description of these states in concert with the problems found in the excitation energy spectrum.

TABLE II. The NCSM ^{10}B, ^{10}Be, and ^{10}C $E2$ transitions, in e^2 fm^4, quadrupole moments, in e fm^2, $M1$ transitions, in μ_N^2, and magnetic moments, in μ_N obtained using the CD-Bonn *NN* potential and the HO frequency $\hbar\Omega = 14$ MeV in the $4\hbar\Omega - 8\hbar\Omega$ basis spaces. Free nucleon charges were used in our calculations. The experimental values are from Ref. [20].

^{10}B	$4\hbar\Omega$	$6\hbar\Omega$	$8\hbar\Omega$	Exp
$Q(3_1^+0))$ [e fm^2]	+6.059	+6.462	+6.799	+8.472(56)
$\mu(3_1^+0)$ [μ_N]	+1.862	+1.857	N/A	+1.8006
$\mu(1_1^+0)$ [μ_N]	+0.850	+0.846	N/A	+0.63(12)
$B(E2;1_1^+0\rightarrow 3_1^+0)$	4.025	4.199	4.512	4.13±0.06
$B(E2;1_2^+0\rightarrow 3_1^+0)$	0.077	0.126	0.163	1.71±0.26
$B(E2;1_2^+0\rightarrow 1_1^+0)$	2.706	3.195	3.742	0.83±0.40
$B(E2;3_2^+0\rightarrow 1_1^+0)$	3.395	4.081	4.754	20.5±2.6
$B(M1;0_1^+1\rightarrow 1_1^+0)$	13.659	13.463	13.345	>1.61
$B(M1;1_2^+0\rightarrow 1_1^+0)$	0.0010	0.0008	N/A	0.0025(4)
$B(M1;1_2^+0\rightarrow 0_1^+1)$	0.271	0.262	0.241	0.197±0.018
$B(M1;2_1^+0\rightarrow 3_1^+0)$	0.0017	0.0013	0.0019	0.0015(3)
$B(M1;2_1^+0\rightarrow 1_1^+0)$	0.0001	0.0001	0.0000	0.011(1)
$B(M1;2_1^+0\rightarrow 1_2^+0)$	0.0255	0.0252	0.0251	0.017(3)
$B(M1;2_1^+1\rightarrow 3_1^+0)$	0.659	0.529	0.457	0.041(4)
$B(M1;2_1^+1\rightarrow 1_1^+0)$	0.045	0.051	0.056	0.32±0.04
$B(M1;2_1^+1\rightarrow 1_2^+0)$	3.283	3.302	3.265	2.86±0.36
$B(M1;2_1^+1\rightarrow 2_1^+0)$	3.722	3.612	N/A	2.50±0.36
$B(M1;2_2^+0\rightarrow 3_1^+0)$	0.064	0.112	0.170	0.050(12)
$B(M1;2_2^+0\rightarrow 1_1^+0)$	0.0000	0.0001	0.0003	0.018(5)
$B(M1;4_1^+0\rightarrow 3_1^+0)$	0.0011	0.0013	0.0013	0.043(7)
^{10}C	$4\hbar\Omega$	$6\hbar\Omega$	$8\hbar\Omega$	Exp
$B(E2;2_1^+\rightarrow 0_1^+)$	4.018	4.913	5.702	12.3±2.0
^{10}Be	$4\hbar\Omega$	$6\hbar\Omega$	$8\hbar\Omega$	Exp
$B(E2;2_1^+\rightarrow 0_1^+)$	5.703	6.080	6.584	10.5±1.1
$B(E2;2_2^+\rightarrow 0_1^+)$	0.087	0.119	0.133	N/A
$B(E2;0_{\rm intr}^+\rightarrow 2_1^+)(E_{0_{\rm intr}^+}$ [MeV])	0.022 (24.76)	0.108(19.93)	0.073(16.99)	3.3±2.0(6.18)
$B(E2;0_{\rm intr}^+\rightarrow 2_1^+)(E_{0_{\rm intr}^+}$ [MeV])	1.315 (31.51)	1.384(25.59)	1.988(22.00)	3.3±2.0(6.18)

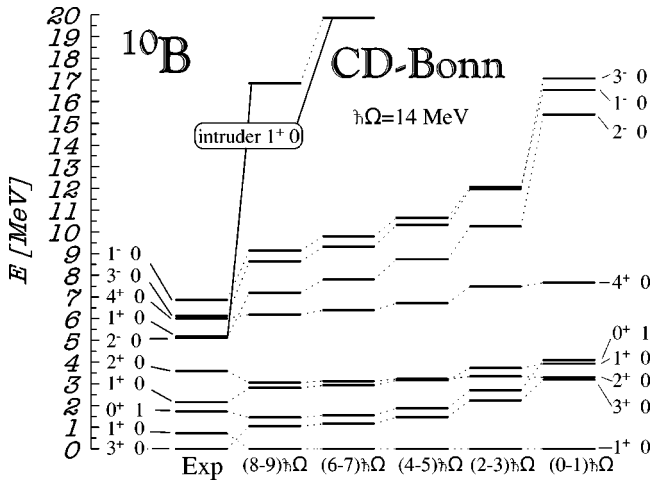

FIG. 5. Experimental and theoretical negative-parity excitation spectra of ^{10}B shown together with selected low-lying positive-parity states including the intruder 1^+0 state. Results obtained in $1-9\hbar\Omega$ model spaces are compared. The calculated excitation energies are obtained by comparing their energies in the $N\hbar\Omega$ space with the ground state in the $(N-1)\hbar\Omega$ space. The effective interaction was derived from the CD-Bonn 2000 *NN* potential in a HO basis with $\hbar\Omega=14$ MeV. The experimental values are from Ref. [20].

We note that for technical reasons the observables in the $8\hbar\Omega$ model space were evaluated using states with $J_z=0$, hence, some observables were not available (the Clebsch-Gordon coefficient being identical to zero).

In Fig. 5, we present the negative-parity energy levels obtained using the CD-Bonn 2000 in basis spaces from the $1\hbar\Omega$ up through the $9\hbar\Omega$. The excitation energies are relative to the $(N-1)\hbar\Omega$ ground states. As with the positive-parity states, we observe a convergence pattern with increasing basis size. This is particularly evident within the negative parity spectrum. On the other hand, the convergence of the overall negative-parity spectrum relative to the positive-parity ground state is somewhat slower than seen for the ground state itself. Nonetheless, even though the negative-parity spectrum is not yet fully converged, it is apparent it will lie higher in excitation than experiment. This is consistent with an overall trend observed in other NCSM calculations, and it is an interesting speculation whether a true tree-body force will be necessary to correct this behavior. We also note that in contrast to the low-lying positive parity states, the level ordering for negative-parity states is in better agreement with the experimental trend.

In addition to the negative-parity states, in Fig. 5 we also exhibit properties of so-called ''intruder'' states, which are characterized with structure dominated by higher $\hbar\Omega$ excitations. Of particular interest to us is the 1^+0 state which we first observe below 20 MeV in the $6\hbar\Omega$ space and drops below 17 MeV in the $8\hbar\Omega$ space. Our calculated intruder state, detailed in Table III, is predominantly a $2\hbar\Omega$ state. This state may be a candidate for the observed 5.18 MeV 1^+0 resonance located just above the ^{6}Li$+\alpha$ threshold. The substantial decrease of the intruder's exciation energy with the basis size contrasts the stability of the $0\hbar\Omega$-dominated states as well as the smooth convergence pattern of the negative-parity $1\hbar\Omega$-dominated states. Significantly larger basis spaces would be needed to obtain convergence of this intruder state.

TABLE III. The NCSM excitation energies, in MeV, and configurations of the two lowest ^{10}B 1^+0 states and the intruder 1^+0 state using the CD-Bonn *NN* potential with Coulomb included. Results obtained in the $6\hbar\Omega$ and $8\hbar\Omega$ basis space using $\hbar\Omega=14$ MeV are presented.

^{10}B $6\hbar\Omega$ basis space					
$J^\pi T$	E_x [MeV]	$0\hbar\Omega$	$2\hbar\Omega$	$4\hbar\Omega$	$6\hbar\Omega$
1^+0	0.0	0.58	0.21	0.13	0.08
1^+0	2.94	0.57	0.21	0.13	0.09
1^+0	19.87	0.02	0.62	0.22	0.14

^{10}B $8\hbar\Omega$ basis space						
$J^\pi T$	E_x [MeV]	$0\hbar\Omega$	$2\hbar\Omega$	$4\hbar\Omega$	$6\hbar\Omega$	$8\hbar\Omega$
1^+0	0.0	0.55	0.19	0.14	0.07	0.05
1^+0	2.82	0.54	0.19	0.14	0.07	0.06
1^+0	16.85	0.02	0.53	0.23	0.13	0.08

B. ^{10}C

The ground-state energy results for ^{10}C are shown in Table I and the HO frequency and basis-size dependence for our CD-Bonn 2000 calculation are shown in Fig. 6. We see from Fig. 6 that with increasing basis size a HO frequency dependence is obtained. Also, the differences between successive curves and energy minima decrease with increasing basis size.

The $B(E2)$ value of the $2_1^+1\rightarrow 0_1^+1$ transition is known experimentally [20], and the result obtained with the CD-Bonn *NN* potential with $\hbar\Omega=14$ MeV is shown in Table II. Our results show steady increase with the basis size, but even in the $8\hbar\Omega$ basis space the experimental value is underestimated considerably, again indicating the need for effective transition operators.

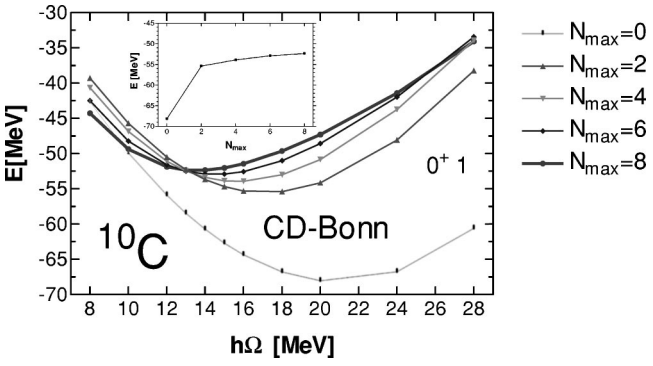

FIG. 6. ^{10}C ground-state energy dependence on the HO frequency for the $0-8\hbar\Omega$ model spaces calculated using the effective interaction derived from the CD-Bonn 2000 *NN* potential. In the inset, the ground-state energies at the HO frequency minima as a function of $N_{\max}$ are plotted.

TABLE IV. Gamow-Teller $B(\mathrm{GT})$ value dependence on the basis-space size for the $^{10}\mathrm{C}(0^+1)\rightarrow{}^{10}\mathrm{B}(1_1^+0)$ transition obtained using the CD-Bonn *NN* potential and the HO frequency $\hbar\Omega = 14$ MeV in the $4\hbar\Omega - 8\hbar\Omega$ basis spaces. The experimental value is from Ref. [21].

$^{10}\mathrm{C}(0^+1)\rightarrow{}^{10}\mathrm{B}(1_1^+0)$	$4\hbar\Omega$	$6\hbar\Omega$	$8\hbar\Omega$	Exp
$B(\mathrm{GT})$	4.847	4.750	4.695	3.44

In Table IV, we compare our calculated $B(\mathrm{GT})$ values for the $^{10}\mathrm{C}(0^+1)\rightarrow{}^{10}\mathrm{B}(1_1^+0)$ transition to experiment. Unlike the $B(E2)$ results, the $B(\mathrm{GT})$ calculations show good stability with respect to the basis-size change, and suggest that the renormalization of Gamow-Teller operator due to the basis truncation should be small. It is interesting to note, though, that we overestimate the experimental value in a similar fashion to results obtained in phenomenological shell-model calculations also performed with free nucleon Gamow-Teller operator reported in Ref. [21].

C. ^{10}Be

Our ground-state energy results for ^{10}Be are shown in Table I and a complete HO frequency and the basis size dependence for our AV8′ calculation is shown in Fig. 7. We make a comprison with the GFMC result [19] obtained using the same *NN* potential. We observe a reasonable agreement similarly as for ^{10}B. As expected from analog symmetry, our calculations for ^{10}Be and ^{10}C are quite similar. Comparing the results in Figs. 6 and 7, we see that the HO frequency, as well as basis size, dependecies are weaker and thus faster convergence is obtained for the CD-Bonn potential in our approach.

Our calculated ^{10}Be excitation spectra are presented in Fig. 8 for the CD-Bonn *NN* potential. As with ^{10}B, selected $B(E2)$ values calculated at the selected HO frequency of $\hbar\Omega = 14$ MeV are listed in Table II.

We also investigated the ^{10}Be negative parity states, and these are shown in Fig. 9 for the CD-Bonn *NN* potential. The

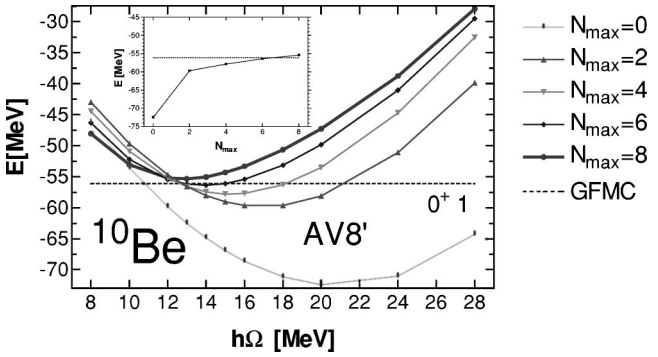

FIG. 7. ^{10}Be ground-state energy dependence on the HO frequency for the $0-8\hbar\Omega$ model spaces calculated using the effective interaction derived from the AV8′ *NN* potential with Coulomb included. The GFMC result is from Ref. [19]. In the inset, the ground-state energies at the HO frequency minima as a function of $N_{\max}$ are plotted.

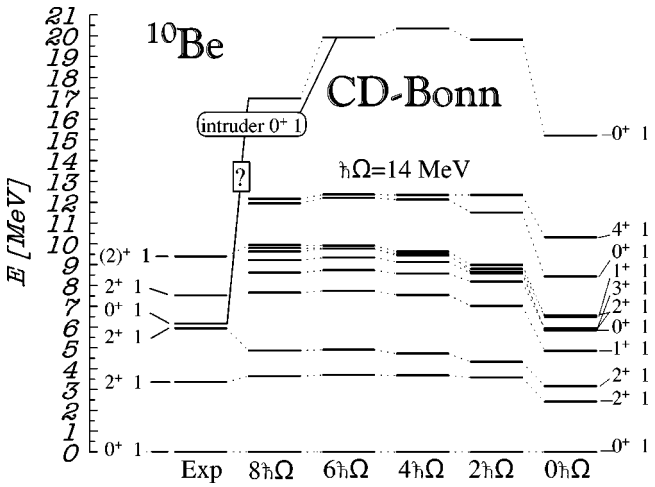

FIG. 8. Experimental and theoretical positive-parity excitation spectra of ^{10}Be. Results obtained in $0-8\hbar\Omega$ model spaces are compared. The effective interaction was derived from the CD-Bonn 2000 *NN* potential in a HO basis with $\hbar\Omega = 14$ MeV. The experimental values are from Ref. [20].

excitation energies obtained in the $1-9\hbar\Omega$ spaces are shown relative to the $(N-1)\hbar\Omega$ ground states. As for the positive-parity states, we observe a convergence pattern where the changes in the excitation energies decrease with increasing basis size. In addition, as with ^{10}B, the overall convergence of the negative parity excitation energies is slower than those with positive parity. It is interesting to note that the level ordering agrees with experiment in all basis spaces, although in the smaller spaces the 0^-1 state lies below the 4^-1. The experimental position of the 0^-1 state is not known and thus we infer that it is likely to lie above the 4^-1 state. We also note that the level spacing improves with

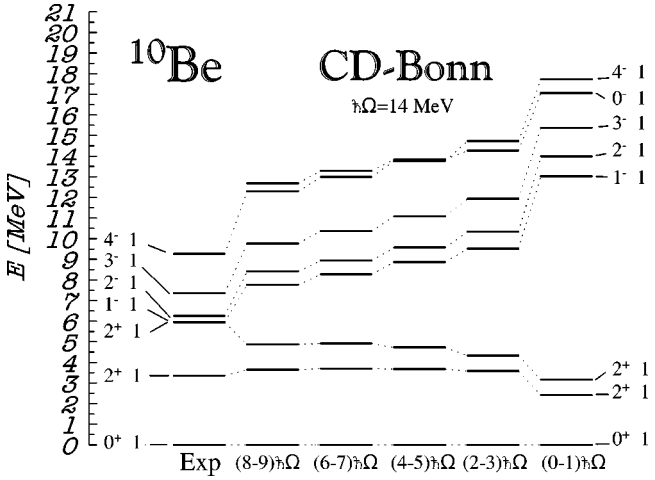

FIG. 9. Experimental and theoretical negative-parity excitation spectra of ^{10}Be shown together with selected low-lying positive-parity states. Results obtained in $1-9\hbar\Omega$ model spaces are compared. The calculated excitation energies are obtained by comparing their energies in the $N\hbar\Omega$ space with the ground state in the $(N-1)\hbar\Omega$ space. The effective interaction was derived from the CD-Bonn 2000 *NN* potential in a HO basis with $\hbar\Omega = 14$ MeV. The experimental values are from Ref. [20].

TABLE V. Gamow-Teller B(GT) value dependence on the basis-space size for the $^{10}\mathrm{B}(3_1^+0)\rightarrow{}^{10}\mathrm{Be}(J^\pi 1)$ transitions obtained using the CD-Bonn *NN* potential and the HO frequency $\hbar\Omega=14$ MeV in the $4\hbar\Omega-6\hbar\Omega$ basis spaces. The experimental values are from Ref. [22].

$^{10}\mathrm{B}(3^+0)\rightarrow{}^{10}\mathrm{Be}(J^\pi 1,\Delta E_{\mathrm{exp}})$	$4\hbar\Omega$	$6\hbar\Omega$	Exp
$B(\mathrm{GT};2_1^+1,3.37)$	0.108	0.124	0.08 ± 0.03
$B(\mathrm{GT};2_2^+1,5.96)$	1.529	1.479	0.95 ± 0.13
$B[\mathrm{GT};(2)^+1,9.4]$	0.122	0.094	0.31 ± 0.08
$B(\mathrm{GT};3^+1)$	0.161	0.176	N/A
$B(\mathrm{GT};4^+1)$	0.0013	0.0021	N/A

the size of the basis compared to experiment. The 2_2^+1 and 1^-1 states have almost the same experimental energy, and in our calculations we underpredict the excitation energy of the 2_2^+1 state and overpredict the 2_1^+1 excitation energy. This is again likely due to an insufficient spin-orbit interaction in the *NN* potentials. At the same time, the calculated excitation energy of the 1^-1 state is too high, and although extrapolations are not straightforward, we expect, based on our experience in lighter systems, that modern *NN* potentials predict the 1^-1 state to be above the 2_2^+1 state. As was the case for ^{10}B, the negative parity states tend to be too high in excitation relative to experiment by 1–2 MeV.

We also evaluated the Gamow-Teller transitions from the ^{10}B 3^+0 ground state to several ^{10}Be states (Table V) and found qualitative agreement with experimental values published in Ref. [22]. At this point, we focus attention on the properties of the spectrum of 0^+ states, as these have bearing on our ability to evalaute the isospin-mixing corrections to the Fermi matrix element in ^{10}C. For this reason, the four lowest 0^+1 states are shown in Fig. 8. In addition, the excitation energies and $\hbar\Omega$ configurations for low-lying 0^+ states, and the first two ''intruder'' states are shown in Table VI. These intruder states are characterized by having significant multi-$\hbar\Omega$ excitations. While both of these intruders are generally $2\hbar\Omega$ in nature, they are in fact quite different. In particular, the lower intruder largely consists of two-particle excitations from the $0p$ shell into the $0s1d$ shell, while the second intruder level is dominated by one-particle $2\hbar\Omega$ excitations. Of these two states, the second has a larger Coulomb matrix element with the ground state (because on average it differs by just one particle), and therefore the analog of this state in ^{10}C and ^{10}B will have a larger effect the isospin-mixing correction to the Fermi matrix element.

Overall, starting at $N_{\mathrm{max}}=2$, the positions of the $0\hbar\Omega$-dominated 0^+1 states are quite stable, which is in contrast to the two ''intruder'' 0^+1 levels whose excitation energies drop dramatically with increasing basis size. This behavior is similar to that of the ''intruder'' states that we recently studied in ^{8}Be with the NCSM [8]. Of considerable importance is the location of these states and their correspondance to experiment. Unfortunately, only two 0^+ states have been identified in ^{10}Be, and there is theoretical speculation [23,24] that the 0_2^+1 state at 6.179 MeV is actually a two-particle excitation intruder state similar to our lower intruder.

TABLE VI. The NCSM excitation energies, in MeV, and configurations of the four lowest ^{10}Be 0^+1 states plus additional 0^+1 intruder states using the CD-Bonn *NN* potential with Coulomb included. Results obtained in the $4\hbar\Omega$, $6\hbar\Omega$, and $8\hbar\Omega$ basis space using $\hbar\Omega=14$ MeV are presented.

		^{10}Be $4\hbar\Omega$ basis space		
$J^\pi T$	E_x [MeV]	$0\hbar\Omega$	$2\hbar\Omega$	$4\hbar\Omega$
0_1^+1	0.0	0.64	0.21	0.15
0_2^+1	9.51	0.66	0.19	0.15
0_3^+1	12.14	0.66	0.19	0.15
0_4^+1	20.35	0.68	0.16	0.16
0_6^+1	24.76	0.01	0.73	0.26
0_8^+1	31.51	0.08	0.67	0.25
		^{10}Be $6\hbar\Omega$ basis space		
$J^\pi T$	E_x [MeV]	$0\hbar\Omega$	$2\hbar\Omega$	$4\hbar\Omega$	$6\hbar\Omega$
0_1^+1	0.0	0.58	0.21	0.13	0.08
0_2^+1	9.78	0.61	0.19	0.12	0.08
0_3^+1	12.26	0.60	0.19	0.13	0.08
0_4^+1	19.93	0.04	0.60	0.22	0.14
0_7^+1	25.59	0.17	0.52	0.17	0.14
		^{10}Be $8\hbar\Omega$ basis space			
$J^\pi T$	E_x [MeV]	$0\hbar\Omega$	$2\hbar\Omega$	$4\hbar\Omega$	$6\hbar\Omega$	$8\hbar\Omega$
0_1^+1	0.0	0.55	0.19	0.14	0.07	0.05
0_2^+1	9.65	0.57	0.18	0.13	0.07	0.05
0_3^+1	11.95	0.56	0.18	0.14	0.07	0.05
0_4^+1	16.99	0.02	0.54	0.23	0.13	0.08
0_6^+1	22.00	0.16	0.45	0.19	0.12	0.08

This state was also studied within cluster models such as, e.g., the molecular orbital model [25] or antisymmetrized molecular dynamics approach [26]. To illustrate the behavior of these intruder states, in Fig. 10 we show the excitation energy of the these states plus the $0\hbar\Omega$-dominated 0_2^+1 state

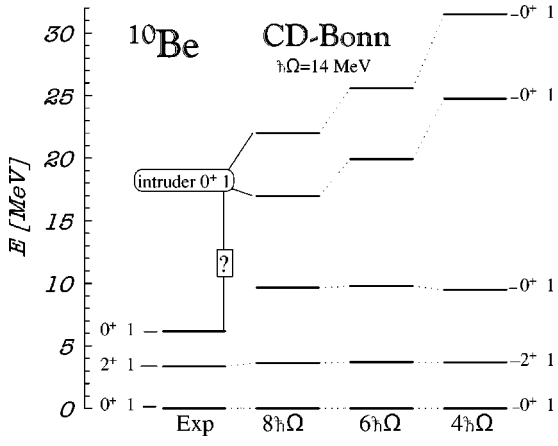

FIG. 10. Experimental and theoretical 2_1^+1, 0_2^+1, and 0^+1 intruder state excitation spectra of ^{10}Be. Results obtained in $4-8\hbar\Omega$ model spaces are shown. The effective interaction was derived from the CD-Bonn 2000 *NN* potential in a HO basis with $\hbar\Omega=14$ MeV. The experimental values are from Ref. [20].

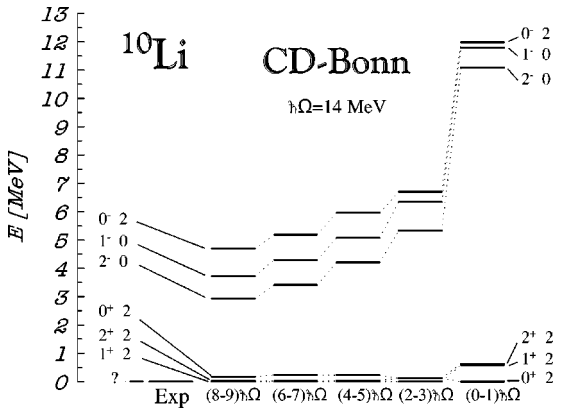

FIG. 11. The calculated lowest-lying positive-parity and negative-parity state excitation energies of ^{10}Li. Results obtained in $0-9\hbar\Omega$ model spaces are compared. The negative-parity excitation energies are obtained by comparing their energies in the $N\hbar\Omega$ space with the ground state in the $(N-1)\hbar\Omega$ space. The effective interaction was derived from the CD-Bonn 2000 *NN* potential in a HO basis with $\hbar\Omega=14$ MeV.

relative to the ground state and the 2_1^+1 level. These are compared with the three corresponding experimental states. It is apparent from the figure that at $8\hbar\Omega$ the two intruders are beginning to exhibit a behavior consistent with convergence, as the rate of change in the excitation energies is decreasing with the larger model spaces. A crude attempt to predict the converged energies based on an exponentially decaying function of $N_{\max}$, as was also done for the intruders in ^{8}Be [8], leads to excitation energies of the order 12.4 and 16.5 MeV for the two intruder levels. At this point it is worth noting that generically we find the excitation energies of the negative-parity, one-particle excitations to be too high by 1–2 MeV. Assuming that this difference is corrected by a three-nucleon force, it is not unreasonable to expect that the excitation energy of the two-particle excitation intruder would be lower still by 2–4 MeV. In addition, with this lower excitation energy, this intruder will start to mix with the $0\hbar\Omega$ state at 9.65 MeV, and will likely lead to a 0_2^+1 state with a lower excitation energy than presently predicted. Unfortunately, at present we are not able to give a further indication as to the nature of the 6.179 MeV state in ^{10}Be.

D. ^{10}Li

The experimental situation is not clear concerning the parity of the ground state of ^{10}Li [27]. We performed the positive- and negative-parity calculations up through $8\hbar\Omega$ and $9\hbar\Omega$ spaces, respectively. As seen in Fig. 11, our results show the positive-parity states lie below the negative-parity states. However, the trend with increasing basis size shows that the negative parity-state binding energies approach quite rapidly the positive-parity state binding energies, and in the largest spaces, the negative-parity states lie within 3 MeV of the positive-parity states. At present, we are not in a position to make a definitive extrapolation and predict the parity of the ^{10}Li ground state for either of the *NN* potentials we employed, but we predict the states of different parity to lie within 1 or 2 MeV. Also, by examining our ^{10}B (Fig. 5) and ^{10}Be (Fig. 9) results, we observe that our $9\hbar\Omega$ states are about 2 MeV above their experimental counterparts. Extrapolating this to our ^{10}Li results, we conclude that the lowest negative- and the positive-parity states of ^{10}Li would be found at approximately the same energy.

We obtain the positive parity 2^+2, 1^+2, and 0^+2 states to be almost degenerate. In the largest space employed $8\hbar\Omega$ we obtain the 1^+2 as the ground state for the CD-Bonn 2000 *NN* potential. We expect that an increase of the spin-orbit interaction due to, e.g., the three-body force would bring the 2^+2 state below the 1^+2 state.

E. ^{10}He

The search for the neutron rich nucleus ^{10}He was reported in Ref. [28]. Our ground-state energy results for ^{10}He obtained for the CD-Bonn 2000 and the AV8′ *NN* potentials are shown in Table I. We observe the smallest difference in our results between the AV8′ and the CD-Bonn compared to the other isobars. However, we note that this could be affected by different convergence rate for the two potentials and a overall slower convergence rate for resonance states in our method.

IV. ISOSPIN-MIXING CORRECTION FOR THE ^{10}C→^{10}B FERMI TRANSITION

Superallowed Fermi β transitions in nuclei $(J^\pi=0^+, T=1)\rightarrow(J^\pi=0^+, T=1)$ provide an excellent laboratory for precise tests of the properties of the electroweak interaction, and have been the subject of intense study for several decades (see Refs. [29–41]). According to the conserved-vector-current (CVC) hypothesis, for pure Fermi transitions the product of the partial half-life, *t*, and the statistical phase-space factor *f* should be nucleus independent and given by

$$ft=\frac{K}{G_V^2|M_F|^2}, \tag{17}$$

where $K/(\hbar c)^6=2\pi^3\ln 2\hbar/(m_e c^2)^5=8.120\,270(12)\times10^{-7}$ GeV^{-4} s, G_V is the vector coupling constant for nuclear β decay, and M_F is the Fermi matrix element, $M_F=\langle\psi_f|T_\pm|\psi_i\rangle$. By comparing the decay rates for muon and nuclear Fermi β decay, the Cabibbo-Kobayashi-Maskawa (CKM) mixing matrix element [34] between *u* and *d* quarks (v_{ud}) can be determined and a precise test of the unitarity condition of the CKM matrix is possible under the assumption of the three-generation standard model [33,34].

For tests of the standard model, two nucleus-dependent corrections must be applied to experimental ft values. The first is a series of radiative corrections to the statistical phase-space factor embodied in the factors δ_R and Δ_R, giving [35–37]

$$f_R=f(1+\delta_R+\Delta_R), \tag{18}$$

where δ_R is due to standard, electromagnetic (''outer'') radiative corrections (see. p. 45 in Ref. [35]) and Δ_R is what has been referred to as the ''inner'' radiative correction (see

p. 47 of Ref. [35]) and includes axial-vector interference terms [37,38]. The second correction, which is the subject of this work, modifies the nuclear matrix element M_F and is due to the presence of isospin-nonconserving (INC) forces (predominantly Coulomb). This correction is denoted by δ_C [30,31,40] and modifies the Fermi matrix element by $|M_F|^2 = |M_{F0}|^2(1-\delta_C)$, where $M_{F0}=[T(T+1)-T_{Z_i}T_{Z_f}]^{1/2}$ is the value of the matrix element under the assumption of pure isospin symmetry.

With the corrections δ_R, Δ_R, and δ_C, a "nucleus-independent" $\mathcal{F}t$ can be defined by

$$\mathcal{F}t = ft(1+\delta_R+\Delta_R)(1-\delta_C), \tag{19}$$

and the CKM matrix element v_{ud} is given by [38]

$$|v_{ud}|^2 = \frac{\pi^3 \ln 2}{\mathcal{F}t}\frac{\hbar^7}{G_F^2 m_e^5 c^4} = \frac{2984.38(6)\ \text{s}}{\mathcal{F}t}, \tag{20}$$

where the Fermi coupling constant G_F is obtained from muon β decay, and includes radiative corrections. Currently, ft values for nine superallowed transitions have been measured with an experimental precision of 0.2% or better [32,42]. With these precise measurements and reliable estimates for the corrections, the CVC hypothesis can be confirmed by checking the constancy of the $\mathcal{F}t$ values for each nucleus, while the unitarity condition of the CKM matrix is tested by comparing the extracted value of v_{ud} with the values determined for $v_{us}=0.2199(17)$ [38] and $v_{ub}<0.0075$ (90% confidence level) [43], i.e., $v^2=v_{ud}^2+v_{us}^2+v_{ub}^2=1$.

For the nine accurately measured cases, the isospin-mixing correction δ_C has been evaluated within the framework of the shell model and split into two components $\delta_C = \delta_{IM}+\delta_{RO}$. The first, δ_{IM}, is due to mixing with low-lying $0\hbar\Omega$ levels within the conventional shell-model space. The second, δ_{RO} accounts for states lying outside the shell-model space, in particular, $1p$-$1h$, $2\hbar\Omega$ excitations, through a mismatch in the radial overlap between the converted proton and neutron in the parent and daughter nuclei, respectively. With these corrections, the unitarity condition of the CKM matrix is found to be 0.9955 ± 0.0017 [44], which represents a three-sigma deviation. Of particular interest is understanding whether the previous estimates of δ_C are somehow flawed due to the decomposition into the two components. In this regard, the NCSM may be able to shed light on this question as both components of δ_C are contained within the same large-scale calculation.

Previously, we applied the no-core shell model wave functions to compute the isospin-mixing correction of the $^{10}\text{C}\rightarrow{}^{10}\text{B}$ Fermi transition [45]. In that study, we were limited to the $4\hbar\Omega$ basis spaces. Also, the formalism used in Ref. [45] was such that full convergence to the exact solution would not be achieved with increasing basis size. In the present paper, we extend our investigations up the $8\hbar\Omega$ space, examine the HO frequency dependence of our results, use a consistent *ab initio* formalism that guarantees convergence to the exact solution, and, finally, use the new CD-Bonn 2000 *NN* potential [11] that includes isospin and charge symmetry breaking in the strong interaction.

TABLE VII. Isospin-mixing correction δ_C, in %, dependence on the basis-space size for the $^{10}\text{C}(0^+1)\rightarrow{}^{10}\text{B}(0^+1)$ Fermi transition. The values correspond to calculations with the ground-state energies at the HO frequency minima at each basis space. The CD-Bonn 2000 *NN* potential was used.

$^{10}\text{C}(0^+1)\rightarrow{}^{10}\text{B}(0^+1)$	$0\hbar\Omega$	$2\hbar\Omega$	$4\hbar\Omega$	$6\hbar\Omega$	$8\hbar\Omega$
δ_C [%]	0.029	0.051	0.068	0.095	0.121

Our goal is to evaluate the Fermi matrix element

$$M_F = \langle {}^{10}\text{B}, 0^+1 | T_- | {}^{10}\text{C}, 0^+1 \rangle, \tag{21}$$

which is equal to $\sqrt{2}$ for an isospin-invariant system. The Fermi matrix element and the correction δ_C was computed using basis spaces ranging from $0\hbar\Omega$ to $8\hbar\Omega$ for a wide range of HO frequncies, i.e., $\hbar\Omega=8$ MeV to $\hbar\Omega=24$ MeV. We quote as our final result the value we obtain in the largest accessible space, i.e., $8\hbar\Omega$, at the HO frequency, where the ground-state energy is at its minimum, i.e., $\hbar\Omega=14$ MeV. However, the trends and dependecies on both $N_{\max}$ and Ω are important to gauge convergence and this motivates this more extensive investigation.

From the point of view of the beta decay of ^{10}C, a good description of the $T=1$ states is important. One measure of our calculations is the coefficients of the isobaric mass multiplet equation (IMME) $[BE(T_z)=a+bT_z+cT_z^2]$. For $A=10$, we find $b=2.365$ MeV and $c=0.535$ MeV, which are to be compared with the experimental values of $b=2.328$ MeV and $c=0.362$ MeV. The larger c-coefficient indicates a somewhat strong isotensor component in the effective interaction. We note, though, that the c coefficient decreases with increasing model space.

The calculated isospin-mixing corrections $\delta_C = 1-|M_F|^2/2$, in %, are presented in Table VII and in Fig. 12. In general, the size of the correction depends on the nuclear radius; the smaller the radius the larger the Coulomb energy and thus the larger the correction. At the same time, the size of the correction also depends on the position of the $1p$-$1h$, $2\hbar\Omega$ states that influence the ground-state isospin

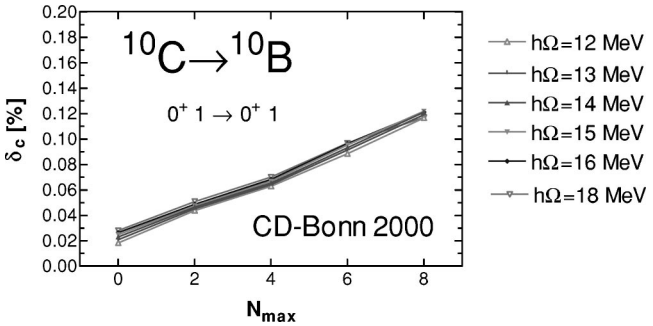

FIG. 12. Isospin mixing correction for the $^{10}\text{C}(0^+1)\rightarrow{}^{10}\text{B}(0^+1)$ Fermi transition as a dependence on the basis size from the $0\hbar\Omega$ to the $8\hbar\Omega$ space for several HO frequencies. The CD-Bonn 2000 *NN* potential was used.

mixing. The lower these states appear, the larger the correction. Unfortunately, the excitation energy of these states is not known experimentally. In our calculations, as a function of the HO frequency $\hbar\Omega$, these two effects cancel to a certain degree because a lower frequency leads to a larger radius but at the same time a lower position of the $1p$-$1h$ states. Consequently, we observe little dependence in δ_C on the HO frequency. On the other hand, we observe a strong dependence in the isospin-mixing correction due to $N_{\max}$. The reason for this strong $N_{\max}$ dependence is the overall decrease in the excitation energy of the $1p$-$1h$, $2\hbar\Omega$ states with increasing basis size discussed in Sec. III C.

It is apparent from both Table VII and Fig. 12 that a saturation in the isospin-mixing correction with increasing basis size is not yet achieved. At present, our best result obtained in the $8\hbar\Omega$ space is $\delta_C = 0.12\%$. This result is compatible with the previously published value of $\delta_C \approx 0.15(9)\%$ by Ormand and Brown [41] obtained in a phenomenological treatment. Also it is compatible with our earlier result published in Ref. [45]. Given the convergence pattern exhibited by the ''intruder'' states discussed in Sec. III C it is likely that δ_C will increase with a larger model space. However, a rough estimate of the full δ_C can be obtained via perturbation theory. The contribution to δ_C due to the $0\hbar\Omega$, 0^+1 states is approximately 0.03% (as shown in Table VII), and, consequently, in the $N_{\max}=8$ model space the contribution of the higher-lying $1p$-$1h$, $2\hbar\Omega$ states is $\approx 0.09\%$. If we assume that all of this contribution can be attributed to the first calcuated $1p$-$1h$ state, an estimate the full value of δ_C would be

$$\delta_C = \left[0.03 + 0.09 \left(\frac{E_x^{8\hbar\Omega}}{E_x^{\text{full}}} \right)^2 \right], \tag{22}$$

where E_x is the excitation energy of the $1p$-$1h$, $2\hbar\Omega$ state in the $8\hbar\Omega$ space and the full model space. In Sec. III C, we arrived at rough estimate of 16.5 MeV for E_x^{full}, leading to $\delta_C \approx 0.19\%$. Note that in some ways this is an overestimate as some fraction of the remaining 0.09% contribution is due to states that lie higher in excitation energy than the first calculated $1p$-$1h$ state. At this point, it is clear that a $10\hbar\Omega$ calculation is desirable to shed more light on the δ_C saturation issue. Such a calculation is likely within reach and may be done in a near future.

Finally, we note that unitarity of the CKM matrix would require a value of 0.58(19) for δ_C [$ft(1+\delta_R+\Delta_R) = 3154 \pm 5.1_{\text{stat}} \pm 2.4_{\text{sys}}$ [46]]. Consequently, although our results are not yet conclusive for a new value of δ_C for the ^{10}C transition, it is unlikely that failure to satisfy the unitarity condition for the CKM matrix is due to a miscalculation, or a missing component, in the previous estimates of the isospin-mixing correction to the Fermi matrix element.

V. CONCLUSIONS

We performed large-scale *ab initio* no core shell model calculations for $A=10$ nuclei with basis spaces up through the $9\hbar\Omega$ with matrix dimensions reaching 5.5×10^8. Using realistic Argonne and CD-Bonn NN potentials, we calculated binding energies, excitation spectra (including negative parity and intruder $2\hbar\Omega$-dominated states), as well as electromagnetic properties and Gamow-Teller transitions.

For ^{10}B, the Argonne and the CD-Bonn NN interactions produce a $J^\pi T = 1^+0$ ground state, contrary to experimentally observed 3^+0 ground state. This is a clear indication of the need for true three-body forces to describe the low-lying structure in complex nuclei. From our ^{10}Li results, we conclude that the lowest negative- and the positive-parity states of ^{10}Li would be found at approximately the same energy. In many ways, the $A=10$ system represents an excellent Laboratory for testing the effects of true three-nucleon forces.

We investigated the isospin-mixing correction of the $^{10}\text{C} \rightarrow {}^{10}\text{B}$ Fermi transition, and obtained $\delta_C = 0.12\%$. However, we expect that this correction will still increase if we were able to access larger basis spaces, and obtain an estimate of 0.19% based on perturbation theory and a rough estimate of the excitation energy of the first $1p$-$1h$, $2\hbar\Omega$ state in the full calculation. Given this modest result and the fact that the unitarity of the CKM matrix would require a value of $\delta_C = 0.58(19)$, it is unlikely that the the breakdown of unitarity in the CKM matrix is due to a miscalculation, or a missing component, in the previous estimates of δ_C.

We note that the NCSM differs from the standard shell model approach, concerning the description of loosely bound states or the isospin-mixing correction, e.g., as used in Ref. [23] or in Ref. [41]. In particular, the standard shell model relies on the assumption that an effective interaction exists and is often determined by tuning to experimental properties. This is also the case for the single-particle properties, where solutions to Woods-Saxon or Hartree-Fock (and sometimes even harmonic oscillator) potentials are used. Again, these are frequently ''tuned'' to experiment by using the appropriate separation energy. In the NCSM approach, on the other hand, no single-particle energies are used and the effective interaction is not emprically determined, but rather derived from the underlying internucleon interaction in a way that guarantees convergence to the exact solution with the basis size enlargement. In the NCSM, it is possible that a precise description of loosely bound and unbound, single-particle resonances, might need a large number of oscillator states; in particular many $\hbar\Omega$, one-particle excitations. This is an important area for future exploration in the NCSM. For the isospin-mixing correction, the primary difference between the NCSM and the standard shell-model approach lies in how low-lying configuration mixing and the radial mismatch are treated. In the standard shell model, these contributions are treated separately, and proton and neutron radial wave functions obtained from an appropriate mean field using experimental separation energies are used (as well as sum over intermediate parent states). On the other hand, both these contributions are accounted for within the NCSM formalism. In particular, the radial-overlap mismatch is primarily described by mixing with higher-lying $2\hbar\Omega$, one-particle excitations by the Coulomb interaction. It is important to note that in addition to the strength of the Coulomb matrix element, the isospin-mixing amplitudes are also determined by the excitation energies of the $2\hbar\Omega$ states. Our study finds

that these excitation energies are also dependent on the model space size, and that although convergence is not yet found some stablization appears to be evident.

We feel that is likely that $10\hbar\Omega$ calculations for $A=10$ nuclei will soon be within reach and are planned for the near future. Such calculations will be interesting for an extended study of the intruder states and the the isospin-mixing correction. In particular, we will re-examine the $^{10}\mathrm{C}\rightarrow{}^{10}\mathrm{B}$ Fermi transition investigation where we need still larger model space results in order to conduct a reasonable extrapolation.

Finally, we make an overall observation. The *ab initio* NCSM with our present theory for H_{eff} and present computer/algorithm/code technologies provide reasonably convergent *p*-shell results for states dominated by $0\hbar\Omega$ configurations. Most other states appear to require, for convergent results, either the use of higher-body effective many-body forces or improved computational capacity, or both. We need and expect additional breakthroughs to access the enlarged range of phenomena where higher than $0\hbar\Omega$ configurations play a major role.

ACKNOWLEDGMENTS

This work was performed in part under the auspices of the U.S. Department of Energy by the University of California, Lawrence Livermore National Laboratory under Contract No. W-7405-Eng-48. P.N. and W.E.O. received support from LDRD Contract No. 00-ERD-028. This work was also supported in part by U.S. DOE Grant No. DE-FG-02-87ER-40371, Division of High Energy and Nuclear Physics.

[1] J.L. Friar, G.L. Payne, V.G.J. Stoks, and J.J. de Swart, Phys. Lett. B **311**, 4 (1993); W. Glöckle and H. Kamada, Phys. Rev. Lett. **71**, 971 (1993); M. Viviani, A. Kievsky, and S. Rosati, Few-Body Syst. **18**, 25 (1995).

[2] B.S. Pudliner, V.R. Pandharipande, J. Carlson, S.C. Pieper, and R.B. Wiringa, Phys. Rev. C **56**, 1720 (1997); R.B. Wiringa, Nucl. Phys. **A631**, 70c (1998); R.B. Wiringa, S.C. Pieper, J. Carlson, and V.R. Pandharipande, Phys. Rev. C **62**, 014001 (2000); S.C. Pieper, V.R. Pandharipande, R.B. Wiringa, and J. Carlson, *ibid.* **64**, 014001 (2001).

[3] P. Navrátil, J.P. Vary, and B.R. Barrett, Phys. Rev. Lett. **84**, 5728 (2000); Phys. Rev. C **62**, 054311 (2000).

[4] D.C. Zheng, B.R. Barrett, L. Jaqua, J.P. Vary, and R.J. McCarthy, Phys. Rev. C **48**, 1083 (1993); D.C. Zheng, J.P. Vary, and B.R. Barrett, *ibid.* **50**, 2841 (1994); D.C. Zheng, B.R. Barrett, J.P. Vary, W.C. Haxton, and C.L. Song, *ibid.* **52**, 2488 (1995).

[5] P. Navrátil and B.R. Barrett, Phys. Rev. C **54**, 2986 (1996); **57**, 3119 (1998).

[6] P. Navrátil and B.R. Barrett, Phys. Rev. C **57**, 562 (1998).

[7] P. Navrátil and B.R. Barrett, Phys. Rev. C **59**, 1906 (1999); P. Navrátil, G.P. Kamuntavičius, and B.R. Barrett, *ibid.* **61**, 044001 (2000).

[8] P. Navrátil, J.P. Vary, W.E. Ormand, and B.R. Barrett, Phys. Rev. Lett. **87**, 172502 (2001); E. Caurier, P. Navrátil, W.E. Ormand, and J.P. Vary, Phys. Rev. C **64**, 051301(R) (2001).

[9] P. Navrátil and W.E. Ormand, Phys. Rev. Lett. **88**, 152502 (2002).

[10] K. Suzuki and S.Y. Lee, Prog. Theor. Phys. **64**, 2091 (1980); K. Suzuki, *ibid.* **68**, 246 (1982).

[11] R. Machleidt, F. Sammarruca, and Y. Song, Phys. Rev. C **53**, 1483 (1996); R. Machleidt, *ibid.* **63**, 024001 (2001).

[12] K. Suzuki, Prog. Theor. Phys. **68**, 246 (1982); K. Suzuki and R. Okamoto, *ibid.* **70**, 439 (1983).

[13] J. Da Providencia and C.M. Shakin, Ann. Phys. (N.Y.) **30**, 95 (1964).

[14] K. Suzuki, Prog. Theor. Phys. **68**, 1999 (1982); K. Suzuki and R. Okamoto, *ibid.* **92**, 1045 (1994).

[15] C.P. Viazminsky and J.P. Vary, J. Math. Phys. **42**, 2055 (2001).

[16] N. Barnea, W. Leidemann, and G. Orlandini, Nucl. Phys. **A650**, 427 (1999).

[17] E. Caurier, G. Martinez-Pinedo, F. Nowacki, A. Poves, J. Retamosa, and A.P. Zuker, Phys. Rev. C **59**, 2033 (1999); E. Caurier and F. Nowacki, Acta Phys. Pol. B **30** 705 (1999).

[18] J. P. Vary, ''The Many-Fermion-Dynamics Shell-Model Code,'' 1992 (unpublished); J. P. Vary and D. C. Zheng, *ibid.*, 1994.

[19] S. Pieper and R.B. Wiringa (in preparation).

[20] F. Ajzenberg-Selove, Nucl. Phys. **A490**, 1 (1988).

[21] W.-T. Chou, E.K. Warburton, and B.A. Brown, Phys. Rev. C **47**, 163 (1993).

[22] I. Daito *et al.*, Phys. Lett. B **418**, 27 (1998).

[23] E.K. Warburton and B.A. Brown, Phys. Rev. C **46**, 923 (1992).

[24] D.J. Millener, Nucl. Phys. **A693**, 394 (2001).

[25] N. Itagaki and S. Okabe, Phys. Rev. C **61**, 044306 (2000).

[26] Y. Kanada-En'yo, H. Horiuchi, and A. Doté, Phys. Rev. C **60**, 064304 (1999).

[27] M. Thoennessen *et al.*, Phys. Rev. C **59**, 111 (1999); J.A. Caggiano, D. Bazin, W. Benenson, B. Davids, B.M. Sherrill, M. Steiner, J. Yurkon, A.F. Zeller, and B. Blank, *ibid.* **60**, 064322 (2000).

[28] J. Stevenson *et al.*, Phys. Rev. C **37**, 2220 (1988); A.N. Ostrowski *et al.*, Phys. Lett. B **338**, 13 (1994).

[29] R.J. Blin-Stoyle, in *Isospin in Nuclear Physics*, edited by D.H. Wilkinson (North-Holland, Amsterdam, 1969), p. 115; D.H. Wilkinson, Phys. Lett. **65B**, 9 (1976); I.S. Towner, S. Raman, T.A. Walkiewicz, and H. Behrens, At. Data Nucl. Data Tables **16**, 451 (1975).

[30] I.S. Towner, J.C. Hardy, and M. Harvey, Nucl. Phys. **A284**, 269 (1977).

[31] W.E. Ormand and B.A. Brown, Phys. Rev. Lett. **62**, 866 (1989)

[32] J.C. Hardy, I.S. Towner, V.T. Koslowsky, E. Hagberg, and H. Schmeing, Nucl. Phys. **A509**, 429 (1990).

[33] A. Sirlin, Rev. Mod. Phys. **50**, 573 (1978).

[34] N. Cabibbo, Phys. Rev. Lett. **10**, 531 (1963); M. Kobayashi and T. Maskawa, Prog. Theor. Phys. **49**, 652 (1973).

[35] R.J. Blin-Stoyle, *Fundamental Interactions and the Nucleus* (North Holland, Amsterdam, 1973).

[36] A. Sirlin and R. Zucchini, Phys. Rev. Lett. **57**, 1994 (1986); W. Jaus and G. Rasche, Phys. Rev. D **35**, 3420 (1987).
[37] W. Jaus and G. Rasche, Phys. Rev. D **41**, 166 (1990); I.S. Towner, Nucl. Phys. **A540**, 478 (1992).
[38] F.C. Barker, B.A. Brown, W. Jaus, and G. Rasche, Nucl. Phys. **A540**, 501 (1992); J.F. Donoghue, B.R. Holstein, and S.W. Klimt, Phys. Rev. D **35**, 934 (1987).
[39] W.E. Ormand and B.A. Brown, Nucl. Phys. **A440**, 274 (1985); W.E. Ormand, Ph.D. thesis, Michigan State University, 1986.
[40] I.S. Towner, in *Symmetry Violation in Subatomic Physics, Proceedings of the 6th Summer Institute in Theoretical Physics*, edited B. Castel and P.J. O'Donnel (World Scientific, Singapore, 1989), p. 211.
[41] W.E. Ormand and B.A. Brown, Phys. Rev. C **52**, 2455 (1995).
[42] G. Savard, A. Galindo-Uribarri, E. Hagberg, J.C. Hardy, V.T. Koslowsky, D.C. Radford, and I.S. Towner, Phys. Rev. Lett. **74**, 1521 (1995).
[43] E.D. Thorndike and R.A. Poling, Phys. Rep. **157**, 183 (1988).
[44] Particle Data Group, D.E. Groom *et al.*, Eur. Phys. J. C **15**, 1 (2000).
[45] P. Navrátil, B.R. Barrett, and W.E. Ormand, Phys. Rev. C **56**, 2542 (1997).
[46] I.S. Towner and J.C. Hardy, in *Proceedings of the V International WEIN Symposium: Physics Beyond the Standard Model*, Santa Fe, NM, edited by P. Herczeg, C.M. Hoffman, and H.V. Klapdor-Kleingrothaus (World Scientific, Singapore, 1999), pp. 338–359.